Journal of the European Ceramic Society 41 (2021) 7105–7110

Contents lists available at ScienceDirect

Journal of the European Ceramic Society

journal homepage: www.elsevier.com/locate/jeurceramsoc

Electric field-assisted synthesis/sintering cerium oxide: 5 wt.% gadolinium oxide

T.C. Porfirio, E.N.S. Muccillo, R. Muccillo *

Center of Science and Technology of Materials – CCTM, Energy and Nuclear Research Institute – IPEN, Travessa R 400, Cidade Universitária, S. Paulo, SP, 05508-170, Brazil

ARTICLE INFO

Keywords:
Cerium oxide
Gadolinium oxide
Electric field-assisted synthesis
Powder consolidation
Sintering

ABSTRACT

Gadolinium oxide ceramic powders were mixed to cerium oxide ceramic powders, pressed to pellets, and sintered either at 1450 °C or applying 200 V cm^{-1} electric field at 800 °C, 900 °C and 1000 °C. The structural phases and the microstructure of the sintered pellets were analyzed by X-ray diffraction and scanning electron microscopy, respectively. The formation of substitutional solid solution was followed by monitoring the increase of the electrical conductivity by impedance spectroscopy and X-ray diffraction. The main results show that Joule heating due to the flow through the pellets of the electric current, which was produced by the application of the electric field, allows for promoting partial solid solution as well as partial sintering the ceria-gadolinia pellets. Moreover, grain growth that occurred in the high temperature sintered pellets was inhibited in the electric field-assisted synthesized/sintered pellets, being an alternative technique for producing cerium oxide-gadolinium oxide solid solutions.

1. Introduction

Gadolinium oxide has been mixed to nuclear fuels to act as burnable (neutron) absorber for enhancing burn out cycles and during recharging nuclear reactors, due to the high neutron cross section of Gd [1]. The preparation process of the neutron absorber consists in mixing 1–10 wt.% Gd_2O_3 to UO_2 ceramic powders, pressing to pellets, and sintering at fairly high temperatures (e.g., 1650 °C–1750 °C) for 2–6 hours to achieve the desired properties. Sintering is performed under controlled reduced atmosphere to obtain ceramic pieces with suitable UO_2 stoichiometry [2–4].

As with the electric field-assisted sintering technique, proposed in 2010 [5], dense ceramic pieces can be produced without grain growth, we decided to perform preliminary experimental work in ceria-gadolinia compounds before applying the technique to uranium dioxide-gadolinium oxide compounds. Ceria was reported to be an appropriate surrogate for uranium dioxide [6]. Moreover, uranium dioxide requires special atmospheres to achieve stoichiometry and handling precautions due to its radioactive behavior.

In conventional sintering, a green pellet is heat treated at a temperature high enough to sinter by solid state reaction of the particles or by a reaction involving liquid phase formation [7–9]. The main parameters to be considered are temperature, dwelling time, heating and cooling rates, and atmosphere. In electric field-assisted sintering (flash sintering when it occurs in short times), on the other hand, the main parameters are electric field amplitude, electric current limit, time the field is applied, and temperature [10–14]. Providing heating by forcing an electric current to flow through a mixture of two or more oxides has already been reported, the authors nominating it flash synthesis when it gives rise to a new compound [15–19].

Many techniques were proposed to synthesize ceria-based electrolytes, for example, combustion [20,21], hydrothermal [22,23], homogeneous precipitation [24], glycine-nitrate process [25], and cation complexation [26].

Flash sintering at temperatures lower than conventional were reported for many oxides [10–14], including two oxides used in the nuclear industry, thorium oxide [27] and uranium oxide [28]. Flash sintering ceria-gadolinia solid solutions were reported using the current-rate method when a dog-bone shaped sample was heated up to 680 °C, achieving full density with 200 mA mm^{-2} [29]. Nanocrystalline ceria-gadolinia powders were synthesized and submitted to experiments leading to submicron grain size with flash sintering at 600 °C [30].

We report here results on sintering a mixture of gadolinium oxide to cerium oxide, either simply by heating to 1450 °C for 4 h (conventional

* Corresponding author.
E-mail addresses: tatiane.porfirio@alumni.usp.br (T.C. Porfirio), enavarro@usp.br (E.N.S. Muccillo), muccillo@usp.br (R. Muccillo).

https://doi.org/10.1016/j.jeurceramsoc.2021.07.027
Received 22 February 2021; Received in revised form 9 July 2021; Accepted 14 July 2021
Available online 17 July 2021

sintering) or by applying 200 V cm^{-1} AC electric field at 800 °C, 900 °C and 1000 °C for 10 min (electric field-assisted pressureless sintering). The main idea was to show that the latter method is cost-effective comparing to the former, and that an extension of the method to a mixture of gadolinium oxide (a neutron absorber) to uranium oxide (a nuclear fuel) may be possible. Noteworthy is that uranium oxide with 5–10 wt.% gadolinium oxide addition has been already used in boiling water reactors for extending burnup. In this case, UO_2-Gd_2O_3 fuel pellets were obtained by high temperature sintering [31].

2. Experimental

Cerium oxide powders (99.9 % CeO_2, Alfa Aesar) were used to prepare mixtures with 5.0 wt.% gadolinium oxide powders (99.98 % Gd_2O_3, Alfa Aesar) by thoroughly mixing in an agate crucible. The mixtures were uniaxially pressed (50 MPa) into disc-shaped pellets with 5 mm diameter and approximately 3 mm thickness, followed by isostatic pressing (140 MPa); the pellets were sintered at 1450 °C/ 4 h in air (10 °C min^{-1} heating and cooling rates) in a Lindberg-Blue M furnace (Watertown, USA) and in a dilatometer DIL 822 (TA Instruments, Hullhorst, Germany) without a dwelling time. The hydrostatic apparent density of the sintered pellets was determined by the Archimedes method in a Mettler Toledo AG-245 (Columbus, USA) analytical balance. The theoretical density value used to determine the relative density was 7.14 g cm^{-3}, obtained from stoichiometric calculations.

Electric field-assisted sintering experiments were performed with the green pellet positioned in the sample holder of a Unitherm 1161V vertical dilatometer (Anter, Pittsburgh, USA), programmed to heat at 10 °C min^{-1} up to 800 °C, 900 °C or 1000 °C for a 10 min dwelling time for application of an electric voltage, and up to 1450 °C for comparison purpose. Dilatometric experiments were performed up to 1000 °C and 1450 °C with a 1 mm thickness fully sintered alumina disk for correction of the dilatometer rod. The dilatometer was modified to have platinum disk electrodes connecting the pellet parallel surfaces to a custom-made power supply (0–55 V, 0–6 A, 0.5–1.2 kHz) via platinum-iridium leads [32]. AC electric voltages of 1 kHz frequency were applied for avoiding electrochemical reduction of the pellets, known to occur when applying DC voltages [33,34].

X-ray diffraction analyses were performed at room temperature in a D8 Advance Bruker-AXS diffractometer (Karlsruhe, Germany) with a θ-2θ Bragg-Brentano configuration using Cu-k_α radiation, 20°-80° and 20°-50° 2θ ranges, 0.05° step size, 5 s per step. EVA® software was used for background correction, subtraction of $k_{\alpha 2}$ contribution, and smoothing of X-ray diffraction patterns. X-ray diffraction analyzes were also performed in the 75°-78° 2θ range, 0.02° step size, 10 s per step, step scan mode, for evaluation of the apparent average crystallite size L using the following equation [35]:

$$L = 0.9\,\lambda / [B(2\theta).\cos(\theta)]$$

where λ is the wavelength of the Cu-k_α radiation (0.15418 nm), B(2θ) is the line broadening at half the maximum intensity in radians, and 2θ is the Bragg angle of the (311) reflection.

Simultaneous thermogravimetric and differential thermal analyses were performed in a Netzsch STA 409E analyzer from room temperature to 1500 °C at 10 °C cm^{-1} rate, under flowing 5 L min^{-1} synthetic air.

Scanning electron microscopy images of surfaces of sintered pellets were obtained in a FEG-SEM Inspect F50 (FEI, Brno, Czech Republic) scanning electron microscope with 10 kV accelerating voltage and 3.0 spot size. The pellets, embedded in a polymeric resin, had one of their parallel surfaces successively polished with 15, 3 and 1 μm diamond paste and thermally etched by inserting the polished pellet into the furnace at 1350 °C during 5 min for revealing the grain structure.

Impedance spectroscopy measurements were carried out for collecting [−Z"(ω) x Z'(ω)] data (Z' and Z" are the real and the imaginary components of the impedance and $f = \omega/2\pi$ is the frequency of the input signal) with a Hewlett Packard 4192A impedance analyzer (Yokogawa-Hewlett Packard, Tokyo, Japan) with 200 mV input signal, 20 points per decade in the 5 Hz-13 MHz frequency range; the samples were spring-loaded between platinum disks inside a custom-made sample chamber made of inconel 600, alumina, and platinum terminal leads connected to the impedance analyzer with two 1 m coaxial cables. Silver paste was deposited on the parallel surfaces of the ceramic pellets and cured at 400 °C/15 min. For the collection of the impedance data, a model 360 Hewlett Packard Controller was used; the collection, analysis, and deconvolution of the [−Z"(ω) x Z'(ω)] impedance diagrams were performed with a special software [36].

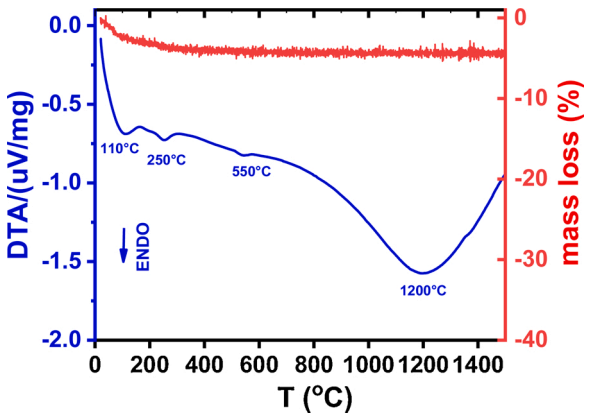

Fig. 1. Thermogravimetric and differential thermal analysis curves of CeO_2 + 5 wt.% Gd_2O_3 ceramic powder.

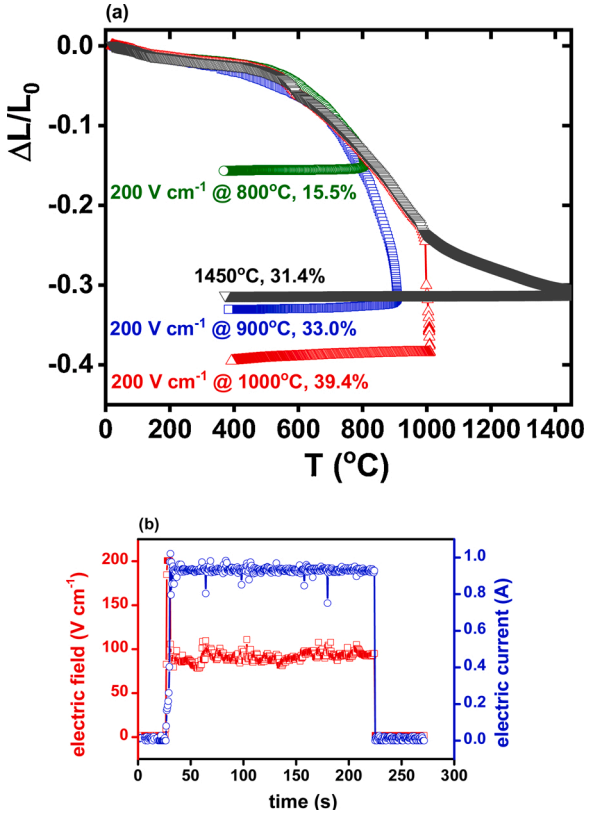

Fig. 2. (a): Dilatometric curves of CeO_2 + 5 wt.% Gd_2O_3 with application for 10 min of 200 V cm^{-1} at 800 °C, 900 °C and 1000 °C and heating up to 1450 °C without application of electric field. The frequency of the applied field and the limiting current were 1 kHz and 1 A, respectively; (b): Typical electric field and current curves during electric field-assisted sintering CeO_2 + 5 wt.% Gd_2O_3.

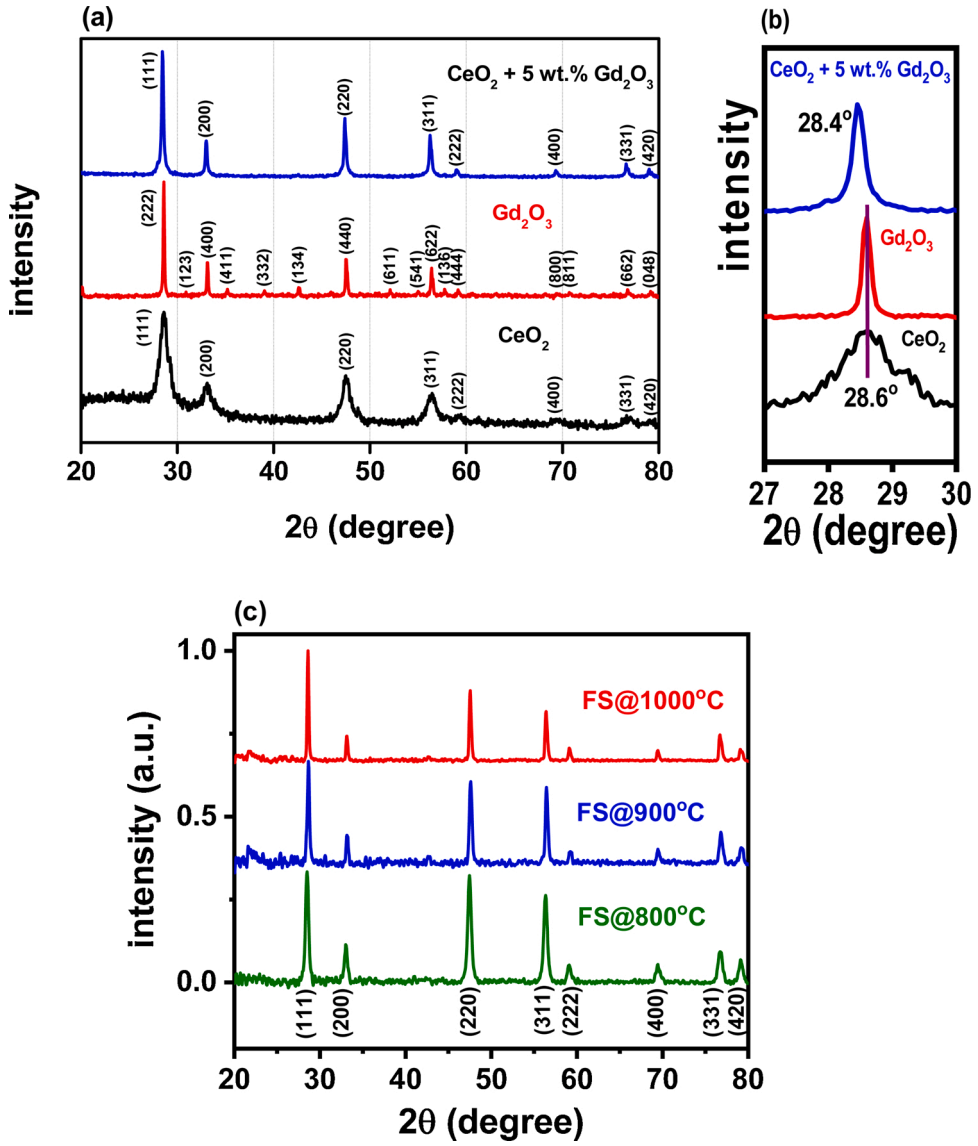

Fig. 3. X-ray diffraction patterns of (a) CeO_2, Gd_2O_3, and CeO_2 + 5 wt.% Gd_2O_3 ceramic powders after heating to 1450 °C/4 h; (b) detail of the [111] reflection of ceria-gadolinia in the 27°-30° 2θ range; CeO_2 + 5 wt.% Gd_2O_3 pellets electric field-assisted sintered at (c) 800 °C/10 min, 900 °C/10 min and 1000 °C/10 min. Miller indices are shown for the reflections of the cubic fluorite structure (ICDD reference pattern n. 75-161).

3. Results and discussion

Fig. 1 shows the simultaneous thermogravimetric and the differential thermal analyses of the CeO_2 + 5 wt.% Gd_2O_3 ceramic powder mixture in the room temperature-1500 °C range. There was no apparent mass gain or loss under flowing synthetic air. The temperature difference between the sample thermocouple and the reference (α-Al_2O_3) thermocouple presents three endothermic peaks at 110 °C, 250 °C, 550 °C, ascribed to losses of impregnated water, structural water, and other ambient-impregnated chemical species (e.g., CO_2) upon handling, respectively [30]. The broad endothermic occurrence with its maximum at 1200 °C might be due to solid solution formation. This is an indication that the thermal energy (Joule heating) provided by electric current derived from the application of the electric voltage in electric field-assisted sintering, must complement the furnace temperature to reach 1200 °C in the sample.

Fig. 2a shows dilatometric curves of cold-pressed pellets of the CeO_2 + 5 wt.% Gd_2O_3 mixture, submitted to pressureless isothermal electric field-assisted sintering: the pellets, positioned in the sample holder of the dilatometer, were heated at 10 °C min^{-1} to 800 °C, 900 °C and 1000 °C. Those temperatures were chosen because there are reports of maximum shrinkage temperature of ceria-gadolinia compounds from 700 °C to 1000 °C, depending on their average particle size [26,37]. Consequently, at those temperatures, a 200 V cm^{-1} electric field was applied during 10 min, resulting in 15.5 %, 33.0 % and 39.4 % thickness reduction, respectively. At the first two temperatures, no detectable effect of the electric field was noticed. However, at 1000 °C, an electric current of approximately 1 A (preset value at the power supply) flowed through the pellet after few seconds, the electric field then decreasing instantaneously to approximately 100 V cm^{-1} to keep the electric current constant at 1 A (see Fig. 2b). Sharp thickness contraction occurred up to 39.4 %, when then the electric voltage was turned off, typical in flash sintering experiments [5,14,38]. The short time elapsed during that thickness reduction was not sufficient for pore elimination (Cf. Fig. 5). The same figure shows also the dilatometric curve up to 1450 °C of a similar pellet, with a final shrinkage level of 31.4 %. Expansion \shrinkage of the dilatometer rod was less than 3% and not taken into account. Flash sintering at 1000 °C promoted larger shrinkage (39.4 %) than sintering to 1450 °C (31.4 %) due to different mechanisms acting in both experiments. Here, we do not deal with sintering ceria-gadolinia

Table 1
Values of lattice parameter and unit cell volume of CeO_2 + 5 wt.% Gd_2O_3 pellets flash-sintered for 10 min at 800 °C, 900 °C, 1000 °C, and sintered at 1450 °C.

Sintering procedure	lattice parameter (±0.00014 Å)	cell volume (±0.0125 Å)
Flash at 800 °C	5.40467	157.8729
Flash at 900 °C	5.40974	158.3176
Flash at 1000 °C	5.41308	158.6113
1450 °C	5.41310	158.6202

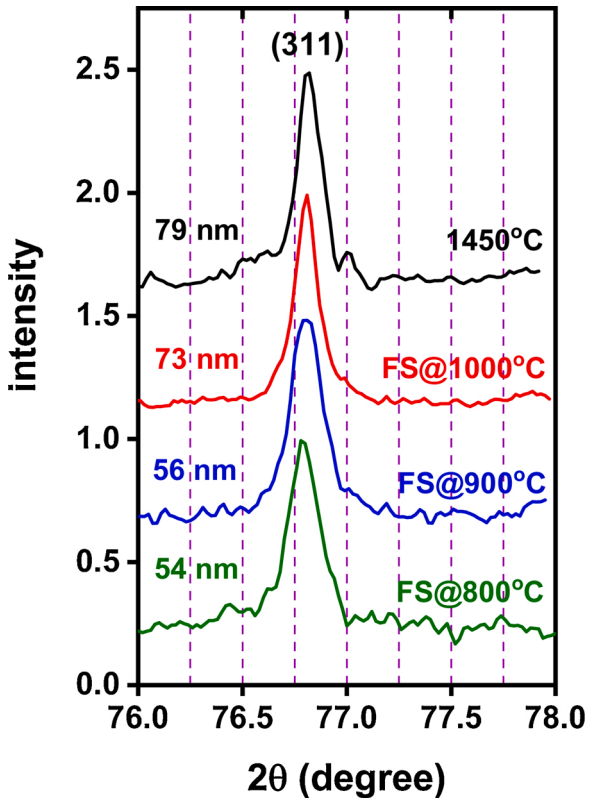

Fig. 4. X-ray diffraction patterns of CeO_2 + 5 wt.% Gd_2O_3 pellets electric field-assisted sintered at (a) 800 °C/10 min, (b) 900 °C/10 min, (c) 1000 °C/10 min, and sintered at 1450 °C, showing the apparent average crystallite size values.

solid solution, but a mixture of ceria and gadolinia powders, with three main competing mechanisms taking part upon heating: (i) sintering of ceria and gadolinia; (ii) solubility of gadolinium ions to the ceria powder, promoting an oxygen vacancy every two gadolinium ions; and (iii) sintering of ceria-5 wt.% gadolinia produced in (ii). One should also consider that in the flash sintering experiment two are the heating sources: Joule heating in the bulk of the pellets and furnace heating at the pellet surfaces. Only the latter applies to conventional sintering. There are several reports that the exposure of cerium oxide to high temperatures leads to Ce^{4+} reduction to Ce^{3+} [39]. That redox reaction is accompanied by the formation of an oxygen vacancy for each pair of Ce^{4+} ions, releasing O_2 and decreasing the density of ceria compounds [39].

The apparent density of CeO_2 + 5 wt.% Gd_2O_3 pellets sintered at 1450 °C for 4 h was evaluated as 98 % T.D. The density of the compact submitted to electric field-assisted sintering was lower, 6.21 g cm^{-3} (~ 70 % T.D.) because the heat produced by the electric current flow in the sample during 10 min was not sufficient to eliminate porosity. However, the grains are welded together due to Joule heating [38,40], providing high skeletal density with improved mechanical stiffness.

Fig. 3 shows the results of the X-ray diffraction measurements of CeO_2 and Gd_2O_3 powders, and of the mixture of these powders (95.0–5.0 wt.%) after pressing and sintering at 1450 °C/4 h (Fig. 3a). The X-ray reflections of the sintered pellet belong to those of the cubic fluorite structure of cerium oxide, with a slight deviation to lower diffraction angle (Fig. 3b), meaning that solid solution was accomplished with Gd^{3+} substituting for Ce^{4+} [41]. Fig. 3c shows the X-ray diffraction patterns of similar pressed pellets after electric field-sintering at 800 °C, 900 °C and 1000 °C. Further evidence of increased solid solution formation for increasing temperature the electric field is applied was found by evaluating the unit cell parameter and volume (Table 1): the lattice parameter increases for increasing sintering temperature:

All XRD peaks of the sintered pellet surfaces can be ascribed to the fluorite cubic phase. The sample sintered by the conventional method has reflections with lower half-width than the electric field-assisted pellets, indicating higher crystallite size. The flash-sintered pellets, on the other hand, show opposite behavior (higher, lower) probably due to their short sintering time (10 min), compared to the dwelling time in the high temperature sintering (4 h). Moreover, no peaks related to Gd_2O_3 are detected.

Fig. 4 shows, for comparison purposes, the (331) reflection of all CeO_2 + 5 wt.% Gd_2O_3 sintered samples, to evaluate the apparent average crystallite sizes following the procedure described by Warren [35]. These values increase for increasing temperature the electric field is applied. The crystallite sizes were 54 nm, 56 nm, 73 nm and 79 nm for samples electric field-assisted sintered at 800 °C, 900 °C, 1000 °C and sintered at 1450 °C without applying the electric field, respectively. As explained before, the sample electric field-assisted sintered at 1000 °C might achieve a temperature T close to 1450 °C to reach similar apparent average crystallite size. The sample temperature T was estimated with the black-body radiation model, which states that $T = [T_0 + W/(S.\sigma)]^{1/4}$; T_0, W, S and σ being the furnace temperature (K), the electric power (voltage times current) dissipated into the sample, the exposed surface area of the sample (m^2), and the Stefan-Boltzmann constant (5.67×10^{-8} W m^{-2} K^{-4}), respectively [5,42,43]. The application of 30 V in a sample with 0.3 cm thickness (100 V cm^{-1}, see Fig. 2b) at 1000 °C in 0.94×10^{-4} m^2 results in 1695 K (1422 °C), in good agreement with the furnace temperature in the conventional sintering (1450 °C).

Fig. 5 shows scanning electron microscopy images of polished and thermally etched surfaces of CeO_2 + 5 wt.% Gd_2O_3 pellets electric field-assisted sintered at 800 °C, 900 °C and 1000 °C (Fig. 5a to c, respectively), and conventionally sintered at 1450 °C for 4 h (Fig. 5d). There is a striking difference between the images of the electric field-assisted sintered pellets and that of the conventionally sintered one: the sample sintered at high temperature, 1450 °C, (Fig. 4d) is dense with close-packed grains with a bimodal pattern with large and relatively small average grain sizes; the samples sintered with the application of electric field at lower temperatures show neck formation, fine grains (submicron size average grain sizes) with slight increase in grain size for increasing temperature the electric field is applied, besides some porosity, in agreement with the evaluated density values.

Fig. 6 shows the results of impedance spectroscopy measurements carried out at 525 °C in the CeO_2 + 5 wt.% Gd_2O_3 electric field-assisted sintered pellets for 10 min at 800 °C, 900 °C and 1000 °C, and in the pellet sintered at 1450 °C in a dilatometer, without application of electric field. The [−Z" x Z'] impedance diagrams of the pellets sintered with application of an electric field at 800 °C, 900 °C and 1000 °C consist of a broad semicircle due to the contribution to the electrical resistivity of bulk (grains) and interfaces (grain boundaries and pores) [44]. The impedance diagram of the pellet sintered at 1450 °C, on the other hand, shows a semicircle at high frequencies due to the electrical resistivity of the grains and a second semicircle due to the contribution of grain boundaries. These considerations agree with the observed scanning electron microscopy micrographs (Fig. 5). The total resistivity of the electric field-assisted sintered pellets decreases from approximately 22 MOhm.cm of the 800 °C sample to 13 MOhm.cm (900 °C) and to 1.5

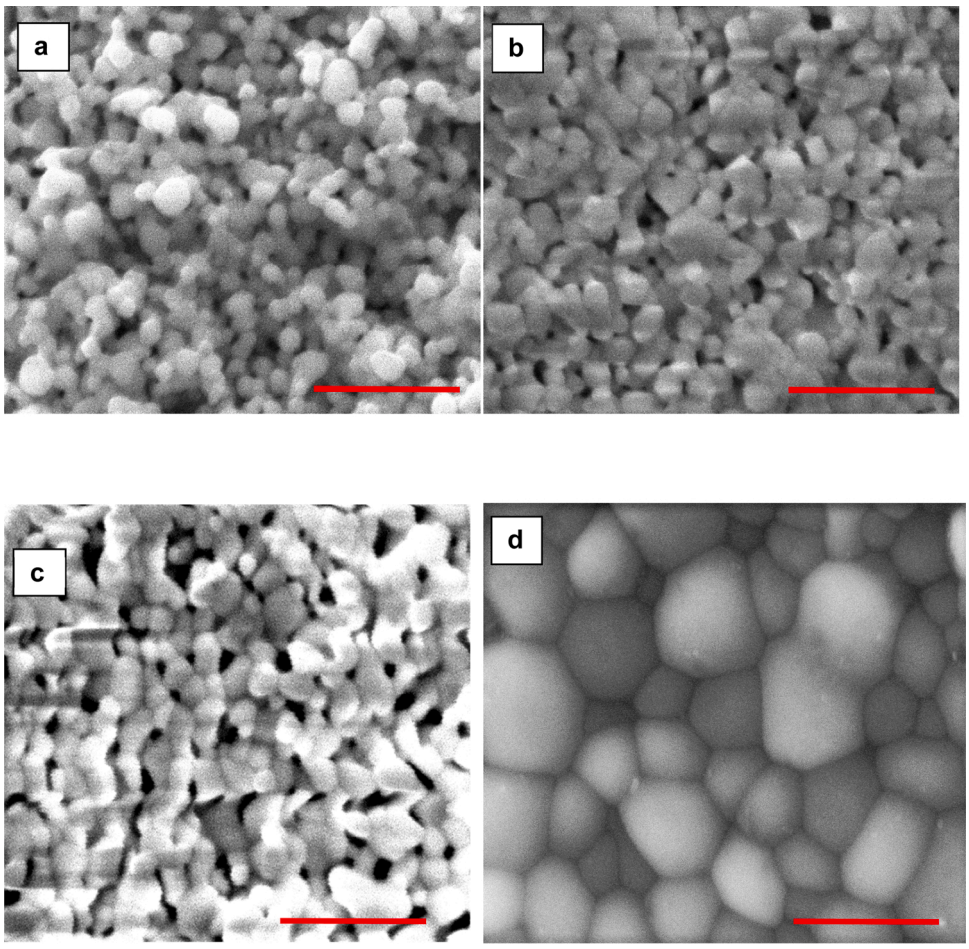

Fig. 5. Scanning electron microscopy images of CeO_2: 5 wt.% Gd_2O_3 pellets electric field-assisted sintered at 800 °C/10 min (a), 900 °C/10 min (b), 1000 °C/10 min (c), and conventionally sintered at 1450 °C/4 h (d). Bar length: 1 μm.

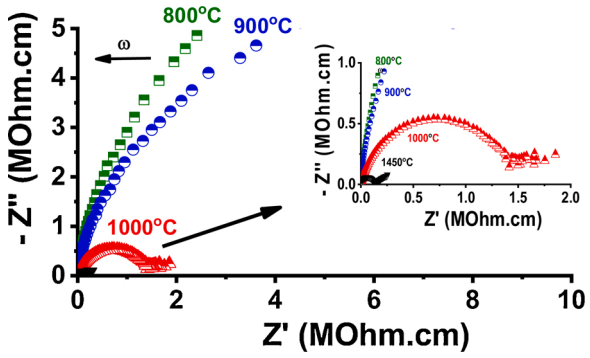

Fig. 6. Impedance spectroscopy diagrams measured at 525 °C in the 5 Hz-13 MHz range of CeO_2 + 5 wt.% Gd_2O_3 pellets electric field-assisted sintered with 200 V cm^{-1} for 10 min at 800 °C, 900 °C and 1000 °C and of pellets sintered at 1450 °C without applying an electric field. Inset: impedance diagrams at the high frequency region.

MOhm.cm (1000 °C) meaning that solid solution has been increasingly formed, enhancing the density of oxygen vacancies and, consequently, decreasing the oxide ion resistivity. The sample sintered at higher temperature without applying the electric field shows much lower ionic resistivity, 0.13 MOhm.cm (see inset in Fig. 6) due to the lower pore density and lower blocking of charge carriers at grain boundaries due to the higher average grain size, as shown in the SEM images of Fig. 5d.

4. Conclusions

Solid solution formation of CeO_2 + 5 wt.% Gd_2O_3 powder mixture were partially accomplished in cold-pressed pellets by application of 200 V cm^{-1} electric field in the 800 °C–1000 °C range during only 10 min. The substitution of Ce^{4+} for Gd^{3+} was ascertained by the evolution of both the X-ray diffraction patterns and the impedance spectroscopy diagrams. Joule heating produced by the electric current, consequence of the application of the electric field, promoted not only partial solid solution of the mixture with increasing temperature, but also sintering. The sintered pellets had exceedingly small grain sizes and higher pore content comparing to samples sintered at 1450 °C for 4 h, leading to relatively higher ionic resistivity values. Further experiments are scheduled for electric field-assisted pressureless sintering these compounds for longer times of applied voltages for improving their density. Moreover, mixtures of uranium dioxide and gadolinium oxide, a burnable neutron absorber, are programmed for electric field-assisted synthesis/sintering under reducing conditions.

Funding

inancial support for this work was provided by Comissão Nacional de Energia Nuclear - CNEN, Fundação de Amparo à Pesquisa do Estado de São Paulo - FAPESP [CINE - Shell (ANP) / FAPESP 2017/11937-4 and CEPID-CDMF 2013/07296-2], and Conselho Nacional de Desenvolvimento Científico e Tecnológico - CNPq (302357/2018-1, 305889/2018-4).

Declaration of Competing Interest

The authors report no declarations of interest.

Acknowledgement

One of the authors (T.C.P.) is grateful to CNEN for the post-doc scholarship.

References

[1] R.A. Murgatroyd, B.T. Kelly, Technology and assessment of neutron absorbing materials, At. Energy Rev. 15 (1977) 3–74. ISSN: 0004-7112.
[2] https://teses.usp.br/index.php?option=com_jumi&fileid=19&Itemid=87&lang=pt-br&g=4&b0=Durazzo&c0=n&o0=AND (In Portuguese).
[3] G. Gunduz, I. Uslu, I. Onal, H.H. Durmazucar, T. Ozturk, A.A. Aksit, B. Kopuz, F. Can, S. Can, R. Uzmen, Effects of different parameters on the densities of uranium-dioxide and uranium dioxide-gadolinium oxide fuels produced by the sol-gel technique, Nuclear Technol. 111 (1995) 63–69, https://doi.org/10.13182/NT95-A35144.
[4] M. Durazzo, H.G. Riella, Effect of mixed powder homogeneity on the UO_2-Gd_2O_3 nuclear fuel sintering behavior, Key Eng. Mater. 189 (2001) 60–66, https://doi.org/10.4028/www.scientific.net/KEM.189-191.60.
[5] M. Cologna, M. Rashkova, R. Raj, Flash Sintering of Nanograin Zirconia in < 5 s at 850°C, J. Am. Ceram. Soc. 93 (2010) 3556–3559, https://doi.org/10.1111/j.1551-2916.2010.04089.x.
[6] S. Patnaik, Comparative analysis of temperature dependent properties of commercial nuclear fuel pellet and surrogates undergoing cracking: a review, Ceram. Int. 46 (2020) 24765–24778, https://doi.org/10.1016/j.ceramint.2020.06.266.
[7] W.D. Kingery, H.K. Bowen, D.R. Uhlmann, Introduction to Ceramics, John Wiley & Sons Inc., 1960. ISBN 978-0-471-47860-47867.
[8] R.M. German, Sintering Theory and Practice, Elsevier Science Ltd., New York, USA, 1982.
[9] R.M. German, Liquid Phase Sintering, Plenum Press, 1985 (1985) ISBN: 978-1-4899-3601-1.
[10] C.E.J. Dancer, Flash sintering of ceramic materials, Mater. Res. Express 3 (2016), 102001, https://doi.org/10.1088/2053-1591/3/10/102001.
[11] M. Yu, S. Grasso, R. McKinnon, T. Saunders, M.J. Reece, Review of flash sintering: materials, mechanisms and modelling, Adv. Appl. Ceram. 116 (2016) 24–60, https://doi.org/10.1080/17436753.2016.1251051.
[12] R. Muccillo, E.N.S. Muccillo, Electric field assisted sintering of electroceramics and in situ analysis by impedance spectroscopy, J. Electroceramics 38 (2016) 24, https://doi.org/10.1007/s10832-016-0054-x.
[13] O. Guillon, C. Elsässer, O. Gutfleisch, F. Janek, S. Korte-Kerzel, D. Raabe, C. A. Volkert, Manipulation of matter by electric and magnetic fields: toward novel synthesis and processing routes of inorganic materials, Mater. Today 21 (2018) 527–536, https://doi.org/10.1016/j.mattod.2018.03.026.
[14] M. Biesuz, V.M. Sglavo, Flash sintering of ceramics, J. Eur. Ceram. Soc. 39 (2019) 115–143, https://doi.org/10.1016/j.jeurceramsoc.2018.08.048.
[15] L.M. Jesus, R.S. Silva, R. Raj, J.C. M'Peko, Electric field-assisted ultrafast synthesis of nanopowders: a novel and cost-efficient approach, RSC Adv. 6 (2016) 107208–107213, https://doi.org/10.1039/C6RA18734J.
[16] E. Gil-Gonzalez, A. Perejon, P.E. Sanchez-Jimenez, M.J. Sayagues, R. Raj, L. A. Perez-Maqueda, Phase-pure $BiFeO_3$ produced by reaction flash-sintering of Bi_2O_3 and Fe_2O_3, J. Mater. Chem. A 6 (2018) 5356–5366, https://doi.org/10.1039/C7TA09239C.
[17] B. Yoon, D. Yadavi, S. Ghose, R. Raj, Reactive flash sintering: MgO and α-Al_2O_3 transform and sinter into single-phase polycrystals of $MgAl_2O_4$, J. Am. Ceram. Soc. 102 (2019) 2294–2303, https://doi.org/10.1111/jace.15974.
[18] B. Yoon, V. Avila, R. Raj, L.M. Jesus, Reactive flash sintering of the entropy-stabilized oxide $Mg_{0.2}Ni_{0.2}Co_{0.2}Cu_{0.2}Zn_{0.2}O$, Scripta Mater. 181 (2020) 48–52, https://doi.org/10.1016/j.scriptamat.2010.02.006.
[19] D. Liu, X. Peng, J. Liu, L. Chen, T. Tang, L. An, Ultrafast synthesis of entropy-stabilized oxide at room temperature, J. Eur. Ceram. Soc. 40 (2020) 2504–2508, https://doi.org/10.1016/j.jeurceramsoc.2020.01.018.
[20] M.M.A. Sekar, S.S. Manoharan, K.C. Patil, Combustion synthesis of fine particle ceria, J. Mater. Sci. Lett. 9 (1990) 1205–1206, https://doi.org/10.1007/BF00721893.
[21] C. Aliotta, L.F. Liotta, V. La Parola, A. Martorana, E.N.S. Muccillo, R. Muccillo, F. Deganello, Ceria-based electrolytes prepared by solution combustion synthesis: the role of fuel on the materials properties, Appl. Catal. B – Environ. 197 (2016) 14–22, https://doi.org/10.1016/j.apcatb.2016.02.044, 0926-3373.
[22] Y.C. Zhou, M.N. Rahman, Hydrothermal synthesis and sintering of ultrafine CeO_2 powders, J. Mater. Res. 8 (1993) 1680–1686, https://doi.org/10.1557/JMR.1993.1680.
[23] M. Hirano, E. Kato, Hydrothermal synthesis of cerium(IV) oxide, J. Am. Ceram. Soc. 79 (1996) 777–780, https://doi.org/10.1111/j.1151-2916.1996.tb07943.x.
[24] N. Uekewa, M. Ueta, Y.J. Wu, K. Kakegawa, Synthesis of CeO_2 spherical fine particles by homogeneous precipitation method with polyethylene glycol, Chem. Lett. 8 (2002) 854–855, https://doi.org/10.1246/cl.2002.854.
[25] C.R. Xia, M.L. Liu, Microstructures, conductivities, and electrochemical properties of $Ce_{0.9}Gd_{0.1}O_2$ and GDC-Ni anodes for low-temperature SOFCs, Solid State Ion. 152 (2002) 423–430, https://doi.org/10.1016/S0167-2738(02)00381-8.
[26] R.A. Rocha, E.N.S. Muccillo, Physical and chemical properties of nanosized powders of gadolinia-doped ceria prepared by the cation complexation technique, Mater. Res. Bull. 38 (2003) 1979–1986, https://doi.org/10.1016/j.materresbull.2003.09.025.
[27] W. Straka, S. Amoah, J. Schwartz, Densification of thoria through flash sintering, MRS Comm. 7 (2017) 677–682, https://doi.org/10.1557/mrc.2017.70.
[28] A.M. Raftery, J.G.P. da Silva, D.D. Byler, D.A. Andersson, B.P. Uberuaga, C. R. Stanek, K.J. McClellan, Onset conditions for flash sintering of UO_2, J. Nuclear Mater. 493 (2017) 264–270, https://doi.org/10.1016/j.jnucmat.2017.06.022.
[29] T.P. Mishra, R.R.I. Neto, R. Raj, O. Guillon, M. Bram, Current-rate flash sintering of gadolinium doped ceria: microstructure and defect generation, Acta Mater. 189 (2020) 145–153, https://doi.org/10.1016/j.actamat.2020.02.036.
[30] L. Spiridigliozzi, M. Biesuz, G. Dell'Agli, E. Di Bartolomeo, F. Zurlo, V.M. Sglavo, Microstructural and electrical investigation of flash-sintered Gd/Sm-doped ceria, J. Mater. Sci. 52 (2017) 7479–7488, https://doi.org/10.1007/s10853-017-0980-2.
[31] Y. Wang, C. Fan, H. Wang, F. Wang, J. Xu, P. Duan, Y. Zhang, Effects of TiO_2 on the sintering densification of UO_2-Gd_2O_3 burnable poison fuel, Ceram. Int. 41 (2015) 10185–10191, https://doi.org/10.1016/j.ceramint.2015.04.124.
[32] R. Muccillo, E.N.S. Muccillo, An experimental setup for shrinkage evaluation during electric field-assisted flash sintering: application to yttria-stabilized zirconia, J. Eur. Ceram. Soc. 33 (2013) 515–520, https://doi.org/10.1016/j.jeurceramsoc.2012.09.020.
[33] H. Conrad, D. Yang, Effect of the strength of an AC electric field compared to DC on the sintering rate and related grain size of zirconia (3Y-TZP), Mater. Sci. Eng. A 559 (2013) 591–594, https://doi.org/10.1016/j.msea.2012.08.146.
[34] C.A. Grimley, A.L.G. Prette, E.C. Dickey, Effect of boundary conditions on reduction during early stage flash sintering of YSZ, Acta Mater. 174 (2019) 271–278, https://doi.org/10.1016/j.actamat.2019.05.001.
[35] B.E. Warren, X-ray Diffraction, Dover Publ. Inc., New York, 1990, p. 254.
[36] M. Kleitz, J.H. Kennedy, Resolution of multicomponent impedance diagrams, in: J. N. Mundy, G.K. Shenoy, P. Vashishta (Eds.), Fast Ion Transport in Solids, Elsevier, North Holland, 1979, pp. 185–188. ISBN-10: 0444003533.
[37] T.H. Santos, J.P.F. Grilo, F.J.A. Loureiro, D.P. Fagg, F.C. Fonseca, D.A. Macedo, Structure, densification and electrical properties of Gd^{3+} and Cu^{2+} co-doped ceria solid electrolytes for SOFC applications: effects of Gd_2O_3 content, Ceram. Int. 44 (2018) 2745–2751, https://doi.org/10.1016/j.ceramint.2017.11.009.
[38] R.I. Todd, E. Zapata-Solvas, R.S. Bonilla, T. Sneddon, P.R. Wilshaw, Electrical characteristics of flash sintering: thermal runaway of Joule heating, J. Eur. Ceram. Soc. 35 (2015) 1865–1877, https://doi.org/10.1016/j.jeurceramsoc.2014.12.022.
[39] Y. Zhou, M.N. Rahaman, Effect of redox reaction on the sintering behavior of cerium oxide, Acta Mater. 45 (1997) 3635–3639, https://doi.org/10.1016/S1359-6454(97)00052-9.
[40] R. Muccillo, M. Kleitz, E.N.S. Muccillo, Flash grain welding in yttria stabilized zirconia, J. Eur. Ceram. Soc. 31 (2011) 1517–1521, https://doi.org/10.1016/j.jeurceramsoc.2011.02.030.
[41] Z. Tianshu, P. Hing, H. Huang, J. Kilner, Ionic conductivity in the CeO_2–Gd_2O_3 system ($0.05 \leq Gd/Ce \leq 0.4$) prepared by oxalate coprecipitation, Solid State Ion. 148 (2002) 567–573, https://doi.org/10.1016/S0167-2738(02)00121-2.
[42] R. Raj, Joule heating during flash-sintering, J. Eur. Ceram. Soc. 32 (2012) 2293–2301, https://doi.org/10.1016/j.jeurceramsoc.2012.02.030.
[43] J.C.C.A. Diaz, R. Muccillo, Liquid-Phase Flash Sintering 8YSZ with Alkali Halide Sintering Aids, J. Eur. Ceram. Soc. 40 (2020) 4299–4303, https://doi.org/10.1016/j.jeurceramsoc.2020.03.022.
[44] M. Kleitz, H. Bernard, E. Fernandez, E. Schouler, Impedance spectroscopy and electrical resistance measurements on stabilized zirconia, in: A.H. Heuer, L. W. Hobbs (Eds.), Advances in Ceramics, Vol. 3, Science and Technology of Zirconia, The Am. Ceram. Soc., Inc., Columbus, OH, 1981, pp. 310–336.